Short-Term Fading Behavior in High-Speed Railway Cutting Scenario: Measurements, Analysis, and Statistical Models

Ruisi He, *Member, IEEE*, Zhangdui Zhong, Bo Ai, *Senior Member, IEEE*, Jianwen Ding, Yaoqing Yang, *Senior Member, IEEE*, and Andreas F. Molisch, *Fellow, IEEE*

***Abstract*—Cuttings are widely used in high-speed railway (HSR) transportation to ensure the flatness of rails. The special structure of cuttings results in rich reflection and scattering, and creates dense multipath components. This paper presents a series of measurements of the propagation channel at 930 MHz conducted along the "Zhengzhou-Xi'an" HSR of China, to characterize the small-scale fading behavior of rail-cutting scenarios as a function of the geometry of cuttings, including crown width and bottom width. Raw data are collected in six cuttings (five cuttings are used for developing the model, while the other one is used for validation) in rural and suburban environments. We propose a set of effective methods to statistically model the spatial/temporal variations – including fade depth (FD), level crossing rate (LCR), average fade duration (AFD), and Ricean K-factor – as a function of the structural parameters of cuttings. Akaike's Information Criterion (AIC)-based evaluation indicates that the Ricean distribution is the best to describe small-scale fading. In addition, the rich multipath and directionality of the transmitting antennas lead to a non-monotonous dependence of the K-factor on the distance between transmitter and receiver. The autocovariance function of the deviation of the extracted K-factors from the proposed model is presented and the coherence length is investigated. Our results show that even though a cutting is a scenario with severe fading, a "wide" cutting (i.e., with both wide crown and bottom widths) is conducive to the reduction of the severity of fading.**

***Index Terms*—Cutting scenario, fading distribution, goodness-of-fit (GoF), high-speed railway (HSR), K-factors, short-term fading behavior.**

I. Introduction

WITHIN the past few decades, high-speed railway (HSR) has been widely introduced to meet the increasing demand for passenger rail travel. HSR becomes more competitive in areas of higher population density due to its faster than normal speed of operation. Meanwhile, a reliable communication system with high capacity and security is a challenging task for HSR [2], [3]. Investigations of radio wave propagation mechanisms and channel modeling are the basis for HSR communication system design and network planning. Unfortunately, to the best of our knowledge, little work has been undertaken to characterize the propagation scenarios that are specific for HSR.

Traditionally, HSR scenarios have been interpreted as standard rural or suburban [3]–[7], because high-speed trains usually travel in such kinds of environments. Based on this interpretation, the classical empirical models such as those of Okumura [8], Hata [9], and Winner [7] are widely used in the engineering implementations of HSR. However, this classification of HSR scenarios is not accurate and can lead to large coverage prediction errors. Based on the measurements obtained from the "Zhengzhou-Xi'an" passenger line [10]–[13], we found that the Hata and Winner models may result in 15 and 20 dB errors for wireless network coverage prediction. This is because the traditional definitions do not take into account the special structures encountered along a railway line, and the restricted set of positions in which the "mobile station" (i.e., the train), can be. For example, HSR requires flatness of tracks to ensure the safety of high-speed trains. Uneven ground, which is acceptable for normal-speed rail, cannot be allowed for HSR construction. These demands introduce some new propagation scenarios [10]–[19], such as cuttings, viaducts, tunnels, etc., whose geometrical layouts are entirely different from standard rural and suburban environments.[1] These special rail structures have significant impacts on propagation characteristics.

Recently, a number of studies have focused on the propagation measurements and analysis in HSR scenarios, especially for viaduct [10]–[13] and tunnel [16]–[19] scenarios. Accurate models for both path loss and fading were obtained for those two scenarios. However, a thorough investigation of a third important class, namely the *cutting scenario* is lacking. Cuttings are used in rail construction on uneven ground, and to help the high speed train pass or "cut" through large obstacles such as hills. By avoiding steep inclines, higher speeds of the train are enabled. A regular deep cutting, where steep walls on both sides of the rails have almost the same depths and slopes, is illustrated in Fig. 1. The cutting sides are usually covered with vegetation and reinforced concrete in case of subsidence. The cutting structure creates a large "container", which can accommodate a great deal

Manuscript received March 25, 2012; revised May 30, 2012; accepted December 03, 2012. Date of publication December 19, 2012; date of current version April 03, 2013. This work was supported in part by the Fundamental Research Funds for the Central Universities under Grant 2012YJS001, Grant 2012YJS004, and Grant2010JBZ008, in part by the National Natural Science Foundation of China under Grant 61222105, and in part by the Beijing Municipal Natural Science Foundation under Grant 4112048.

Part of this paper was presented at IEEE Globecom'2012 [1].

R. He, Z. Zhong, B. Ai, and J. Ding are with the State Key Laboratory of Rail Traffic Control and Safety, Beijing Jiaotong University, Beijing 100044, China (e-mail: ruisi.he@ieee.org).

Y. Yang is with the Department of Computer and Electronics Engineering, University of Nebraska-Lincoln, Omaha, NE 68182 USA (e-mail: yyang3@unl.edu).

A. F. Molisch is with the Department of Electrical Engineering, University of Southern California, Los Angeles, CA 90089 USA (e-mail: Andreas.Molisch@ieee.org).

Color versions of one or more of the figures in this paper are available online at http://ieeexplore.ieee.org.

Digital Object Identifier 10.1109/TAP.2012.2235399

[1]In fact the original HSR environments (i.e., the original state of the environment, for example, the original suburban structure) are mostly destroyed by rail construction.

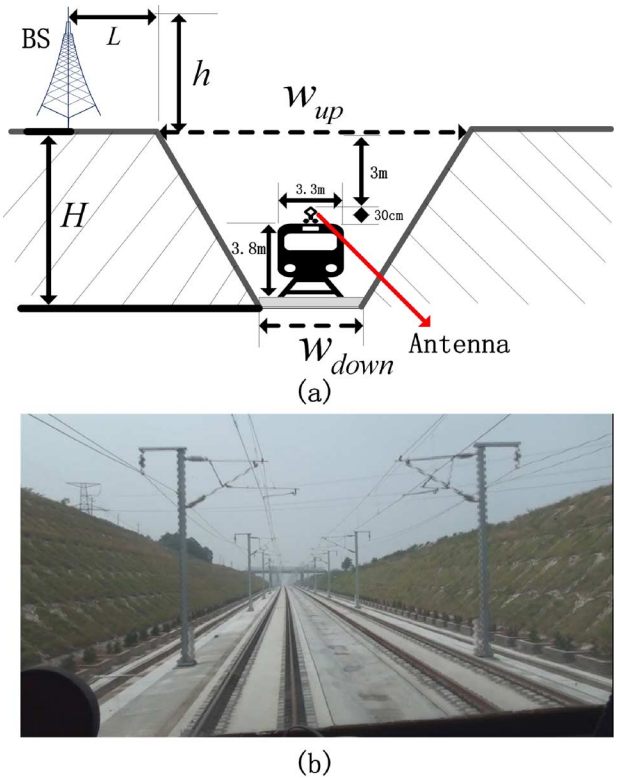

Fig. 1. Sectional view of (a) a deep cutting, and (b) a representative of a real deep cutting scenario. The cutting sides are usually covered with vegetation and reinforced concrete in case of subsidence.

of reflection and scattering components. In HSR environments, the receiver antenna is generally lower than the upper eave of the cutting, which increases the possibility for multipath components to be received. While HSR is a typical line-of-sight (LOS) propagation scenario, where the direct ray usually provides the dominant component of the received signal, the many multipath components reflected or scattered by the sidewalls can lead to severe fading. Therefore, a cutting has a significant impact on radio wave propagation characteristics, providing the motivation for investigating it in this paper.

Generally, two main problems are encountered in the investigation of propagation [20]–[22]: 1) variations due to path loss and shadowing occur over relatively large distances, and b) signal variations due to spatial/temporal changes of multipath interference occur over very short distances. The latter is usually considered as small-scale fading behavior and has been studied by numerous papers in different (non-railway) environments [23]–[25]. References [26], [27] have proposed some empirical large scale models in the cutting scenario, however, the fading analysis is incomplete due to the limited measurements and failure to consider structural parameters. [14] considers an HSR cutting as an open area with low reflection, which is not strictly accurate as discussed above. Thus, an in-depth investigation of small-scale fading is still absent for cutting scenarios. The current paper aims to fill this gap.

We focus on some typical fading parameters: fade depth (FD), level crossing rate (LCR), average fade duration (AFD), and fading distributions. Our data are collected from the measurements taken along a practical HSR, covering six cuttings with different structures. Furthermore, an effective method is proposed to develop statistical models for these fading parameters. We find that some of these fading parameters depend on the structures of the cuttings. Then, the proposed models are validated through measurements. Finally, we summarize the impact of the rich reflection and scattering components on small-scale fading behavior, and discuss the optimal structure of cutting to reduce the severity of fading.

The paper is organized as follows: The measurement campaigns are described in Section II. The method for developing statistical models is provided in Section III. The analysis results and statistical models of the temporal variations are presented in Section IV. The proposed models are validated in Section V. The impact of structural parameters are fully discussed in Section VI. Finally, the conclusions are given in Section VII.

II. Measurements

A. Measurement System

We conducted a series of narrowband measurements at 930 MHz operation frequency along the "Zhengzhou-Xi'an" HSR of China. The detailed descriptions of the test system are as follows.

- Transmitter: Existing GSM base stations for railways are utilized as transmitters. They are usually positioned 15 m (L in Fig. 1) away from the cutting, and have a 28 m antenna height h above ground in our measurements. The broadcast control channel signal with a carrier frequency of 930 MHz is fed to the base station antenna as the transmission signal. The output power of the transmitter is 43 dBm, connected to the cross-polarization directional antennas (pointed along the track) with 17 dBi gain and 65° horizontal and 6.8° vertical beam widths.
- Receiver antenna: The high-speed train in our test is 204 m long, 3.8 m high, and 3.3 m wide. The omnidirectional receiver antennas are placed in the front part of a train car, mounted on the top at a height of 30 cm above the roof of the train, and with a gain of 4 dBi.
- Other equipment: We use a Willtek 8300 Griffin fast measurement receiver to collect and save power data. A distance sensor is set on a wheel of the locomotive to record wheel speed. Under the location-trigger mode, sampling of the Griffin receiver can change with the velocity of the train with the help of the distance sensor, so that the spatial sampling interval is fixed no matter how fast the train moves. The measurement locations are accurately resolved with a GPS (global positioning system) receiver.

We took data snapshots every 10 cm, and took repeated measurements in each cell to collect sufficient samples for study of the fading behavior, as shown in Table I. The sampling intervals were less than half of the wavelength to provide sufficient statistics for extraction of the short-term fading parameters. The effects of slow fading were removed by averaging using a sliding/overlapped window with a step size of one wavelength and a window size of 40 wavelengths[2] in accordance with

[2]A general principle of choosing the segment is that the segment should be as short as possible (to preserve wide-sense stationarity within the window) but long enough for getting a "good" number of independent samples. 40 wavelengths ($\approx$ 13m at 930 MHz) windowing has been suggested for HSR [29], [30], and is widely used in the HSR engineering implementation.

TABLE I
PARAMETERS OF CUTTING NO. 1 TO 6

	Cutting Number	1	2	3	4	5	6
Structural Parameters (m)	w_{up}	58.30	50.86	52.01	55.26	55.72	53.93
	w_{down}	15.16	16.85	18.77	18.57	18.25	14.78
	H	7.1	7.1	7.1	7.1	7.1	7.1
	h	28	28	28	28	28	28
Measurement Parameters	Cellular radius (m)	1332	1013	667	689	1421	1410
	Sampling interval (cm)	10	10	10	10	10	10
	Repeated measurements	4	3	3	3	3	4
	Average speed (km/h)	260	290	295	133	72	260

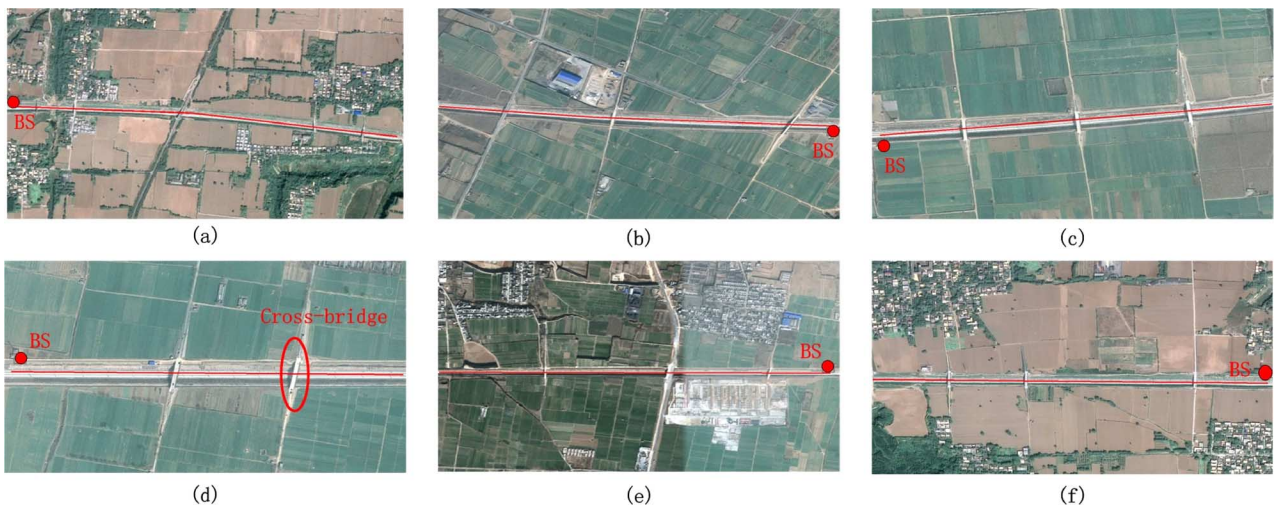

Fig. 2. Aerial view of each cutting. The red solid points indicate the locations of the base stations, and the red lines indicate the railway tracks. A cross-bridge in cutting No. 4 is marked using a red ellipse as an example. (a) Cutting No. 1. (b) Cutting No. 2. (c) Cutting No. 3. (d) Cutting No. 4. (e) Cutting No. 5. (f) Cutting No. 6.

previous suggestions for macrocells [28]–[30]. The lowest average signal-to noise ratio (SNR) measured at a particular location is approximately 30 dB, while higher values are measured in most locations.

B. Measurement Scenario

We chose six deep cuttings along the HSR track to investigate the small-scale fading behavior, and we numbered them 1 to 6. Note that Nos. 1 to 5 are used for parameterization of the fading behavior and No. 6 is used for the model validation. Structural parameters of each cutting are summarized in Table I. The crown width w_{up} and bottom width w_{down} of each cutting were recorded. The values of w_{up}'s and w_{down}'s in Table I are the average values, based on measurements taken at five different locations of each cutting. Since most deep cuttings in HSR have a nearly fixed H,[3] our analysis only analyzes the impact of w_{up} and w_{down}. Note that even those parameters are not fully considered by other existing literature [14], [26] [27]. Our subsequent analysis investigates the impact of these structural parameters on the statistical models of fading parameters. We stress that we have the fixed H, h, and L (as shown in Fig. 1) in the measurements of all six cutting scenarios, to ensure that the positions and heights of base stations do not affect our parameterization.

Aerial views of the six cuttings are shown in Fig. 2. HSR tracks are usually placed in two kinds of environments.

- Suburban environments, where the buildings are typically low residential or townhouses with one or few floors. Occasional uncluttered areas make the environment rather open. Vegetation is modest [7], as the cuttings No. 1, No. 5, and No. 6 shown in Fig. 2. For HSR lines, most vegetation and buildings are 300 m away from the rail tracks.
- Rural environments, where there is a large range of open area, as in the cuttings No. 2, No. 3, and No. 4, shown in Fig. 2. For HSR lines, few buildings exist around the track. Most of the vegetation adjacent to the track is crops with a height of less than 2 m.

These six cuttings cover typical propagation environments for HSR. Note that there are no obstructions to block the LOS path in the cutting scenarios, except occasional cross-bridges as marked in Fig. 2. The comparison of cutting scenarios between suburban environments (Nos. 1, 5, and 6) and rural environments (Nos. 2, 3, and 4) allows us to study the impact of the surrounding obstacles. The different structural parameters of these six cuttings help to develop and validate the statistical models of fading behavior.

[3]Note that $H = 7.1$ m in Fig. 1 is a typical case. The actual value of H changes essentially from 7 to 8 m in our measurements. We stress that the receiver antenna is always lower than the upper eave of the cuttings in our measurements, which means the shallow cuttings are not considered in this paper. Under these circumstances, the accuracy of our models is not sensitive to the minor fluctuations of H in the measurements. More arguments can be found in Section VI.

III. Statistical Modeling Method

In this section, we describe the proposed statistical method to model the temporal variations as a function of the structural parameters of the cuttings. The basic idea of our strategy is to model the impact of each structural parameter on the fading statistics by using a least mean square error (LMSE) regression fit, and then to select the most suitable expression by using a goodness-of-fit (GoF) test.

To start out, we define two sets

$$W = \Big\{ w_{\mathrm{up}},\ w_{\mathrm{down}},\ w_{\mathrm{up}} + w_{\mathrm{down}},\ w_{\mathrm{up}} - w_{\mathrm{down}},\ w_{\mathrm{up}} w_{\mathrm{down}},\ \frac{w_{\mathrm{up}}}{w_{\mathrm{down}}} \Big\} \quad (1)$$

$$V = \big\{ \mathrm{FD},\ a_{\mathrm{LCR}},\ b_{\mathrm{LCR}},\ c_{\mathrm{LCR}},\ a_{\mathrm{AFD}},\ b_{\mathrm{AFD}},\ c_{\mathrm{AFD}},\ k_1,\ k_2,\ k_3,\ \sigma \big\}. \quad (2)$$

W [shown as (1)] is a collection of the structural parameters of cuttings[4] and their combinations – addition, subtraction, multiplication, and division; and V (shown as (2)) is a collection of the key small-scale fading parameters of radio channels and coefficients of the models which are widely accepted to be strongly affected by the physical properties of the environments. The elements of V will be defined in Section IV. The models that consider the channel parameters as a function of the environments (e.g., structural parameters of cuttings) are of great importance to the channel simulation. Therefore, not only the statistical results of small-scale fading parameters are obtained, but they are also developed as the models of the structural parameters, which can be expressed as

$$v = F(w) \quad (3)$$

where $v \in V$, $w \in W$, and $F(\bullet)$ is a function of the undetermined model of v and w. Implementation of the modeling of a certain variable v is shown in Fig. 3:

First, we determine the most suitable functional form to approximate the dependence of v on w_1. We define five simple functions $\tilde{F}_j$ for $j = 1, \ldots 5$, namely $\tilde{F}_1(w_1) = a\log_{10}(w_1)+b$, $\tilde{F}_2(w_1) = a\sqrt{w_1}+b$, $\tilde{F}_3(w_1) = aw_1+b$, $\tilde{F}_4(w_1) = a(w_1)^2+b$, and $\tilde{F}_5(w_1) = ae^{bw_1}$. For each $\tilde{F}_j(w_1)$ its undetermined coefficients a and b are calculated by the LMSE regression fit (these coefficients depend on j, but for notational convenience this dependence is not written explicitly). The reason we use these five functions can be found in Appendix A. We then perform a GoF test on each of those five functions (to increase reliability, we actually perform three GoF tests, namely the sum of squared errors (SSE), R-Square, and root mean squared error (RMSE), whose calculations can be found in Appendix B; as we will show later on, the results from the three tests are consistent with each other), and determine the functional fit $\tilde{F}_{\hat{j}(1)}(w_1)$ that performs best (among all functions $\tilde{F}_j$ according to the GoF criterion. We furthermore test whether $\tilde{F}_{\hat{j}(1)}(w_1)$ passes the GoF test in an absolute sense (i.e., leads to a result that the GoF test accepts[5]; if not, $\tilde{F}_{\hat{j}(1)}(w_1)$ is discarded later.

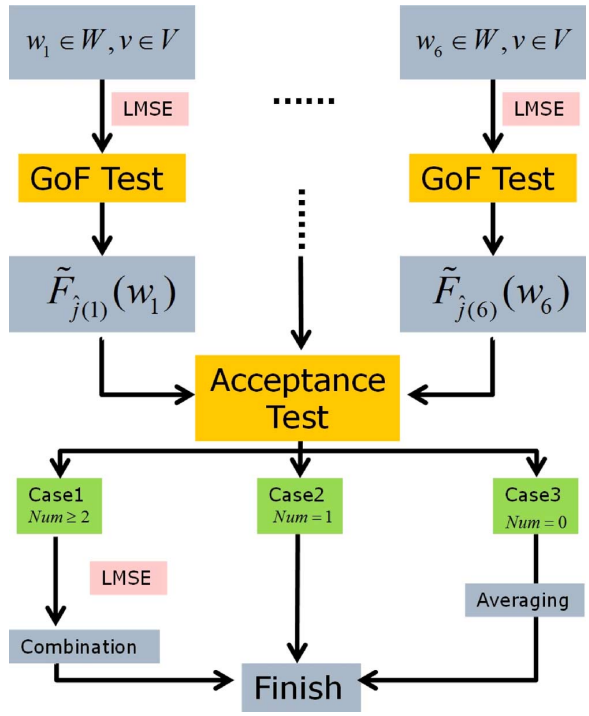

Fig. 3. Flowchart describing the statistical modeling methodology to investigate the effect of the structural parameters of cuttings on the fading behavior.

Second, we conduct the similar operation for other elements of W (i.e., $w_2, w_3 \ldots, w_6$): for each w, we select one suitable function $\tilde{F}(\bullet)$ from the five fitting functions as a candidate to predict v. We thus obtain a set of up to 6 functions $\tilde{F}_{\hat{j}(i)}(w_i)$, $\mathrm{i} = 1, \ldots 6$. The actual number of accepted fits is denoted as *Num*. More precisely, let $\mathcal{I}$ denote the set of all i for which $\tilde{F}_{\hat{j}(i)}(w_i)$ is accepted in the GoF test; then *Num* is the cardinality of $\mathcal{I}$. Remember that each w_i can increment $\mathcal{I}$ by at most one element.

Third, we define a composite model for F from the functional fits for the individual i. For this definition, we have to distinguish three cases

- Case 1: $Num \geq 2$, which means there are more than one $\tilde{F}_{\hat{j}(i)}(w_i)$ that indicate a good model fit. In this case, we model $F(\bullet)$ as a linear combination of all the well-fitting functions. In this case we use the following linear combination:

$$v = \sum_{i \in \mathcal{I}} p_i \tilde{F}_{\hat{j}(i)}(w_i) \quad (4)$$

  where the weight coefficients p_i's can be calculated using an LMSE regression fit[6].

[4]The height H of cuttings is not considered as a structural parameter in the modeling. This is because we have a nearly fixed H in our six cuttings. The elements of W cover the most typical environment parameters in HSR cutting scenarios; compare Section VI.

[5]The threshold of acceptance is defined in Appendix B.

[6]Note the danger of over fitting in this model, i.e., the number of fitting parameters could exceed the number of observation values. In that case the number of functions used in the linear combining should be reduced. The problem does not occur in our particular setup because *Num* never exceeds 2, as we will see in the subsequent sections

- Case 2: $Num = 1$. We assume that the model $\tilde{F}_{\hat{j}(i)}(w_i)$ gives the best fit.
- Case 3: $Num = 0$, which means that v is fairly independent of structural parameters, or has a functional dependence not well modeled by our test functions. Consequently, a reasonable value of v for a cutting scenario is the average value based on all the measurements[7], which is a constant and can be expressed as $v = \left(\sum_{n=1}^{N} v_n\right)/N$, where v_n indicates the measured v in the n-th cutting, N indicates the number of cuttings used for the parameterization, which is 5 in this paper.

Even though the selection of the suitable model from all the candidate functions is somewhat complicated, this modeling approach has many benefits: 1) it uses the LMSE regression fit and GoF test, which can be easily implemented using some well-known software tools such as Matlab, 2) the calculation is very fast, 3) the models developed with this approach can ensure sufficient accuracy for our subsequent analysis. The drawback is that the relatively few measurements can only provide limited data for the LMSE regression fit, which reduces the category of the candidate functions that we can consider. Despite this drawback, the analysis in Section V shows that the accuracy of the developed models is quite good.

In the next section, we will present the small-scale fading behavior derived from the measurements and the statistical modeling using the method in Fig. 3.

IV. Results

A. Fade Depth

Fade Depth (FD) measures the variation in the signal energy about its local mean due to small scale fading. It is an important channel parameter from the perspective of system design as it determines the required fade margin and link budget for an acceptably low system outage probability [22]. FD is defined as the difference in power levels (in decibels) between the 50% and 1% level values for each case [31]. We obtain the 50% and 1% values from the empirical cumulative distribution function (CDF), as shown in Fig. 4. The results of FD are summarized in Table II. It is found that the FD for the cutting scenario is around 17 dB, which is close to the 18.5 dB obtained for Rayleigh fading. This is a result of the steep walls on both sides of the cutting. They retain the reflection and scattering components and lead to severe small-scale fading.

Next, we develop the statistical model for FD by using the method in Section III:

1) We first model FD with $w_{\rm up}$ using the five simple functions mentioned in Section III. The LMSE regression fit leads us to the five formulations: $\mathrm{FD} = -17.76\log_{10}(w_{\rm up}) + 48.23$, $\mathrm{FD} = -2.07\sqrt{w_{\rm up}} + 32.66$, $\mathrm{FD} = -0.14w_{\rm up} + 24.92$, $\mathrm{FD} = -0.0012(w_{\rm up})^2 + 21.09$, and $\mathrm{FD} = 27.05e^{-0.0081w_{\rm up}}$.

[7]As an alternative approach, we also tested the combination of the two structural parameters with the highest R-Square (using an expression similar to (4)) even if they did not pass the GoF test. While this approach in some cases gave better GoF results than the constant (average) value, it did not provide acceptable quality either, and so the additional complexity of using this method was not warranted.

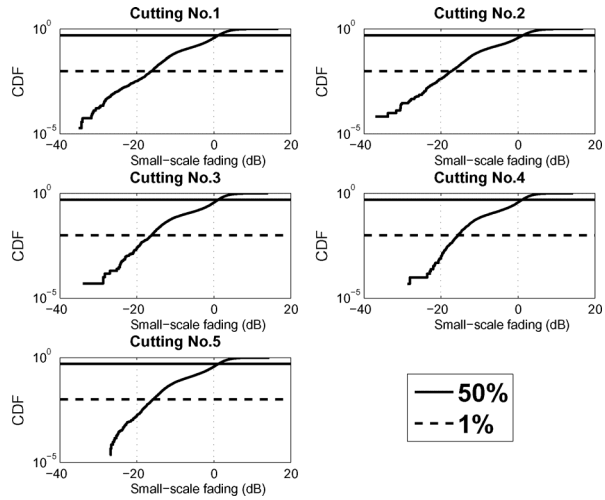

Fig. 4. CDF of the measured small-scale fading for each cutting based on multiple measurements.

2) We determine which of the five functions is the most suitable choice by using the GoF test. It shows that $\mathrm{FD} = -17.76\log_{10}(w_{\rm up}) + 48.23$ should be used, with the smallest SSE at 1.16 and largest R-Square at 0.38. However, we also see that this function does not pass the GoF test, and thus should not be part of the final composite fit.
3) Then, we use the similar method as in 1) and 2) to examine the other structural parameters. The best fit function for each structural parameter is summarized in Table III[8], which can be used to develop the final model of FD.
4) Table III shows that both $w_{\rm up} + w_{\rm down}$ and $w_{\rm up}w_{\rm down}$ model FD quite well with the accepted GoF statistics. The R-Squares of both are close to each other and are both fairly high (> 0.7). This means that both $w_{\rm up} + w_{\rm down}$ and $w_{\rm up}w_{\rm down}$ are responsible for the variation of FD. Therefore, the appropriate expression of FD should be a combination of the two well-fitting functions.

Finally, we carry out the regression fit using a linear combination (suggested in Case 1 of Fig. 3), and the results lead us to the formulation

$$\mathrm{FD(dB)} = 25.26e^{-0.013(w_{\rm up}+w_{\rm down})} + 11.49e^{-0.00045(w_{\rm up}w_{\rm down})}. \quad (5)$$

The GoF statistics of this model are: $\mathrm{SSE} = 0.091$, $\mathrm{R\text{-}Square} = 0.95$, and $\mathrm{RMSE} = 0.17$. Obviously, (5) presents a small prediction error and explains the variation of the data successfully. It shows that even in a small variation range of FD, the structural parameters of cutting still significantly affect the fading behavior. The formulation also implies that the "wide" cutting (with great $w_{\rm up} + w_{\rm down}$ and $w_{\rm up}w_{\rm down}$) results in few received reflected and scattered waves from the steep walls, and considerably reduces the severity of fading.

[8]Note that for space reasons, Table III only displays (for each w_i) the function that is the selected one from the five fitting functions. Then they are used for the comparison to develop the final model.

TABLE II
ANALYSIS RESULTS OF EACH CUTTING

	Cutting Number	1	2	3	4	5
Fading Depth	FD (dB)	17.43	18.53	17.37	16.79	16.94
LCR(crossings) per wavelength	10 dB	0.011	0.0199	0.0123	0.0089	0.0084
	0 dB	0.721	0.751	0.629	0.718	0.751
	-10 dB	0.220	0.250	0.189	0.206	0.206
	-20 dB	0.011	0.012	0.0079	0.0025	0.0055
AFD (wavelengths)	10 dB	95.15	50.06	81.25	112.1	118.73
	0 dB	0.517	0.493	0.573	0.505	0.496
	-10 dB	0.319	0.326	0.382	0.331	0.326
	-20 dB	0.306	0.312	0.315	0.311	0.307
Results of v's	a_{LCR}	0.91	0.95	0.76	0.90	0.95
	b_{LCR}	0.16	0.15	0.17	0.18	0.18
	c_{LCR}	-0.23	-0.21	-0.23	-0.24	-0.24
	a_{AFD}	0.42	0.43	0.54	0.44	0.42
	b_{AFD}	0.021	0.02	0.032	0.022	0.021
	c_{AFD}	0.54	0.50	0.43	0.49	0.63
	k_1	0.0245	0.033	0.0316	0.0143	0.032
	k_2	3.851	1.643	4.519	3.078	2.934
	k_3	-0.00382	-0.001	-0.00811	-0.00331	-0.00164
	σ (dB), $d \leq 200$ m	4.88	4.41	4.89	4.14	3.92
	σ (dB), $d > 200$ m	4.24	4.55	4.38	4.51	4.57

TABLE III
GOODNESS-OF-FIT EVALUATIONS

$v \in V$	$w \in W$	SSE	R-Square	RMSE	Evaluation	$v \in V$	$w \in W$	SSE	R-Square	RMSE	Evaluation
FD (dB)	$\mathrm{FD} = -17.76\log_{10}(w_{\mathrm{up}}) + 48.23$	1.16	0.38	0.62		a_{LCR}	$a_{\mathrm{LCR}} = 0.57e^{0.0083w_{\mathrm{up}}}$	0.023	0.080	0.087	
	$\mathrm{FD} = -0.0062(w_{\mathrm{down}})^2 + 19.3$	1.49	0.21	0.70			$a_{\mathrm{LCR}} = -0.00065(w_{\mathrm{down}})^2 + 1.1$	0.020	0.18	0.082	
	$\mathrm{FD} = 45.11e^{-0.013(w_{\mathrm{up}}+w_{\mathrm{down}})}$	0.28	0.85	0.31	Accepted		$a_{\mathrm{LCR}} = 0.000019(w_{\mathrm{up}}+w_{\mathrm{down}})^2 + 0.8$	0.024	8.2e-3	0.090	
	$\mathrm{FD} = -0.66\sqrt{w_{\mathrm{up}} - w_{\mathrm{down}}} + 21.39$	1.72	0.091	0.76			$a_{\mathrm{LCR}} = 0.7\log_{10}(w_{\mathrm{up}} - w_{\mathrm{down}}) - 0.2$	0.021	0.16	0.083	
	$\mathrm{FD} = 26.57e^{-0.00045(w_{\mathrm{up}}w_{\mathrm{down}})}$	0.43	0.77	0.38	Accepted		$a_{\mathrm{LCR}} = -0.54\log_{10}(w_{\mathrm{up}}w_{\mathrm{down}}) + 2.49$	0.023	0.060	0.088	
	$\mathrm{FD} = 0.053\frac{w_{\mathrm{up}}}{w_{\mathrm{down}}} + 17.24$	1.87	1.0e-3	0.79			$a_{\mathrm{LCR}} = 0.6\log_{10}(\frac{w_{\mathrm{up}}}{w_{\mathrm{down}}}) + 0.6$	0.020	0.17	0.082	
b_{LCR}	$b_{\mathrm{LCR}} = 0.2\log_{10}(w_{\mathrm{up}}) - 0.18$	5.9e-4	0.13	0.014		a_{AFD}	$a_{\mathrm{AFD}} = -0.000071(w_{\mathrm{up}})^2 + 0.66$	8.8e-3	0.20	0.054	
	$b_{\mathrm{LCR}} = 0.088e^{0.037w_{\mathrm{down}}}$	3.5e-4	0.39	0.011			$a_{\mathrm{AFD}} = 0.00056(w_{\mathrm{down}})^2 + 0.28$	7.6e-3	0.31	0.050	
	$b_{\mathrm{LCR}} = 0.0037(w_{\mathrm{up}} + w_{\mathrm{down}}) - 0.099$	2.8e-4	0.79	0.010	Accepted		$a_{\mathrm{AFD}} = -0.0035(w_{\mathrm{up}} + w_{\mathrm{down}}) + 0.70$	0.011	0.033	0.059	
	$b_{\mathrm{LCR}} = -0.00001(w_{\mathrm{up}} - w_{\mathrm{down}}) + 0.2$	7.0e-4	1.57e-5	0.015			$a_{\mathrm{AFD}} = -0.7\log_{10}(w_{\mathrm{up}} - w_{\mathrm{down}}) + 1.5$	7.4e-3	0.32	0.050	
	$b_{\mathrm{LCR}} = 0.00017w_{\mathrm{up}}w_{\mathrm{down}} + 0.010$	2.15e-5	0.97	2.7e-3	Accepted		$a_{\mathrm{AFD}} = 0.41\log_{10}(w_{\mathrm{up}}w_{\mathrm{down}}) - 0.79$	0.01	0.081	0.058	
	$b_{\mathrm{LCR}} = -0.0016(\frac{w_{\mathrm{up}}}{w_{\mathrm{down}}})^2 + 0.18$	6.0e-4	0.11	0.014			$a_{\mathrm{AFD}} = -0.56\log_{10}(\frac{w_{\mathrm{up}}}{w_{\mathrm{down}}}) + 0.72$	7.3e-3	0.33	0.049	
c_{LCR}	$c_{\mathrm{LCR}} = -0.33\log_{10}(w_{\mathrm{up}}) + 0.34$	3.5e-4	0.41	0.011		b_{AFD}	$b_{\mathrm{AFD}} = -0.00062w_{\mathrm{up}} + 0.057$	8.5e-5	0.14	5.3e-3	
	$c_{\mathrm{LCR}} = -0.0001(w_{\mathrm{down}})^2 - 0.2$	4.9e-4	0.19	0.013			$b_{\mathrm{AFD}} = 0.0056e^{0.081w_{\mathrm{down}}}$	7.1e-5	0.28	4.9e-3	
	$c_{\mathrm{LCR}} = -0.0042(w_{\mathrm{up}} + w_{\mathrm{down}}) + 0.07$	7.6e-5	0.87	0.005	Accepted		$b_{\mathrm{AFD}} = -0.0002(w_{\mathrm{up}} + w_{\mathrm{down}}) + 0.04$	9.7e-5	0.016	5.7e-3	
	$c_{\mathrm{LCR}} = -0.1\log_{10}(w_{\mathrm{up}} - w_{\mathrm{down}}) - 0.1$	5.3e-4	0.12	0.013			$b_{\mathrm{AFD}} = 0.071e^{-0.03(w_{\mathrm{up}}-w_{\mathrm{down}})}$	7.3e-5	0.26	4.9e-3	
	$c_{\mathrm{LCR}} = -0.00014w_{\mathrm{up}}w_{\mathrm{down}} - 0.010$	1.5e-4	0.75	0.007	Accepted		$b_{\mathrm{AFD}} = 0.041\log_{10}(w_{\mathrm{up}}w_{\mathrm{down}}) - 0.1$	9.0e-5	0.088	5.5e-3	
	$c_{\mathrm{LCR}} = 0.0013\log_{10}(\frac{w_{\mathrm{up}}}{w_{\mathrm{down}}}) - 0.23$	6.0e-4	3.3e-5	0.014			$b_{\mathrm{AFD}} = -0.049\log_{10}(\frac{w_{\mathrm{up}}}{w_{\mathrm{down}}}) + 0.047$	7.1e-5	0.28	4.9e-3	
k_1	$k_1 = 0.43e^{-0.051w_{\mathrm{up}}}$	1.9e-4	0.26	7.9e-3		c_{AFD}	$c_{\mathrm{AFD}} = 1.74\log_{10}(w_{\mathrm{up}}) - 2.5$	0.017	0.29	0.076	
	$k_1 = -0.00023w_{\mathrm{down}} + 0.031$	2.5e-4	2.0e-3	9.1e-3			$c_{\mathrm{AFD}} = -0.0003(w_{\mathrm{down}})^2 + 0.61$	0.023	0.040	0.088	
	$k_1 = -0.0017(w_{\mathrm{up}} + w_{\mathrm{down}}) + 0.15$	1.7e-4	0.32	7.5e-3			$c_{\mathrm{AFD}} = 0.064e^{0.029(w_{\mathrm{up}}+w_{\mathrm{down}})}$	0.018	0.25	0.078	
	$k_1 = 0.083e^{-0.03(w_{\mathrm{up}}-w_{\mathrm{down}})}$	2.1e-4	0.14	8.5e-3			$c_{\mathrm{AFD}} = 0.88\log_{10}(w_{\mathrm{up}} - w_{\mathrm{down}}) - 0.9$	0.018	0.26	0.077	
	$k_1 = -0.000038(w_{\mathrm{up}}w_{\mathrm{down}}) + 0.063$	2.2e-4	0.14	8.6e-3			$c_{\mathrm{AFD}} = 0.38e^{0.00032(w_{\mathrm{up}}w_{\mathrm{down}})}$	0.024	0.027	0.089	
	$k_1 = -0.03\log_{10}(\frac{w_{\mathrm{up}}}{w_{\mathrm{down}}}) + 0.042$	2.4e-4	0.041	8.9e-3			$c_{\mathrm{AFD}} = 0.54\log_{10}(\frac{w_{\mathrm{up}}}{w_{\mathrm{down}}}) + 0.26$	0.021	0.14	0.083	
k_3	$k_3 = 0.012\log_{10}(w_{\mathrm{up}}) - 0.025$	3.1e-5	0.011	3.2e-3		k_2	$k_2 = 15.57\log_{10}(w_{\mathrm{up}}) - 23.81$	4.12	0.12	1.17	
	$k_3 = -0.000048e^{0.24w_{\mathrm{down}}}$	2.7e-5	0.15	3.0e-3			$k_2 = 0.0032(w_{\mathrm{down}})^2 + 2.22$	4.57	0.023	1.23	
	$k_3 = -0.01\log_{10}(w_{\mathrm{up}} + w_{\mathrm{down}}) + 0.02$	3.2e-5	3.8e-3	3.1e-3			$k_2 = 0.41(w_{\mathrm{up}} + w_{\mathrm{down}}) - 25.38$	2.14	0.82	0.61	Accepted
	$k_3 = 0.014\log_{10}(w_{\mathrm{up}} - w_{\mathrm{down}}) - 0.03$	3.0e-5	0.050	3.1e-3			$k_2 = 0.00082(w_{\mathrm{up}} - w_{\mathrm{down}})^2 + 2.07$	4.43	0.052	1.22	
	$k_3 = -0.019\log_{10}(w_{\mathrm{up}}w_{\mathrm{down}}) + 0.052$	3.0e-5	0.057	3.1e-3			$k_2 = 10.35\log_{10}(w_{\mathrm{up}}w_{\mathrm{down}}) - 27.62$	4.13	0.12	1.17	
	$k_3 = 0.013\log_{10}(\frac{w_{\mathrm{up}}}{w_{\mathrm{down}}}) - 0.01$	2.9e-5	0.065	3.1e-3			$k_2 = 0.056(\frac{w_{\mathrm{up}}}{w_{\mathrm{down}}})^2 + 2.65$	4.58	0.021	1.24	
σ(dB)	$\sigma = -0.93\log_{10}(w_{\mathrm{up}}) + 6.07$	0.76	2.6e-3	0.50		σ(dB)	$\sigma = -0.00021(w_{\mathrm{up}})^2 + 5.07$	0.059	0.24	0.14	
	$\sigma = -5\log_{10}(w_{\mathrm{down}}) + 10.67$	0.61	0.20	0.45			$\sigma = 2.15\log_{10}(w_{\mathrm{down}}) + 1.78$	0.049	0.36	0.13	
	$\sigma = -0.046(w_{\mathrm{up}} + w_{\mathrm{down}}) + 7.77$	0.69	0.082	0.48			$\sigma = -1.75\log_{10}(w_{\mathrm{up}} + w_{\mathrm{down}}) + 7.7$	0.074	0.044	0.16	
$d \leq$ 200m	$\sigma = 3.88e^{0.0037(w_{\mathrm{up}}-w_{\mathrm{down}})}$	0.74	0.021	0.50		$d >$ 200m	$\sigma = -0.033(w_{\mathrm{up}} - w_{\mathrm{down}}) + 5.76$	0.038	0.72	0.10	Accepted
	$\sigma = -0.003(w_{\mathrm{up}}w_{\mathrm{down}}) + 7.32$	0.54	0.29	0.42			$\sigma = 3.88e^{0.00015(w_{\mathrm{up}}w_{\mathrm{down}})}$	0.067	0.13	0.15	
	$\sigma = 0.058(\frac{w_{\mathrm{up}}}{w_{\mathrm{down}}})^2 + 3.87$	0.65	0.14	0.47			$\sigma = -0.035(\frac{w_{\mathrm{up}}}{w_{\mathrm{down}}})^2 + 4.8$	0.039	0.47	0.11	

B. LCR and AFD

LCR and AFD are used to determine how often the received signal crosses (in the positive direction) a given threshold per time unit, and for how long on average the signal is below a certain threshold. They can help in the selection of transmission bit rates, word lengths, and interleaving algorithm [32]. For example, the AFD determines the average length of error bursts in fading channels. Hence, long data blocks are more likely to be affected by the channel with large AFD than short blocks. This should be kept in mind for choosing the frame length for coded packetized systems, designing interleaved or non-interleaved concatenated coding methods [33], etc.. Therefore, we need empirical formulas for the LCR and AFD to design HSR communication systems.

In this paper, LCR is normalized and given in terms of crossings per wavelength, whereas AFD is also given in terms of wavelength, as in [32]. The results of LCR and AFD for four typical threshold levels (R) are tabulated in Table II. It is found that for $R = 0$ dB, there are nearly 7 crossings in an observation window of 10 wavelengths, whereas for $R = -20$ dB, there are just a few crossings in an observation window of 1000 wavelengths. As to AFD, fade duration on average lasts for 0.52 wavelengths at $R = 0$ dB in an observation window of 1 wavelength, and for $R = -20$ dB, the values of AFD are close to 0.31 wavelengths.

We then model LCR and AFD using the data with the thresholds from -20 dB to 10 dB. For LCR, we choose the following expression[9] based on an LMSE test similar to the one in Fig. 3

$$\mathrm{LCR} = \begin{cases} a_{\mathrm{LCR}} e^{b_{\mathrm{LCR}} R} & -20\ \mathrm{dB} \le R \le 0\ \mathrm{dB} \\ a_{\mathrm{LCR}} e^{c_{\mathrm{LCR}} R} & 0\ \mathrm{dB} < R \le 10\ \mathrm{dB} \end{cases}. \quad (6)$$

The undetermined coefficients a_{LCR}, b_{LCR}, and c_{LCR} are summarized in Table II. First, we use the method in Fig. 3 to model a_{LCR} with structural parameters. Table III shows that none of these models indicate good fit, therefore, the average value is chosen: $\bar{a}_{\mathrm{LCR}} = 0.89$. Second, we find that both $w_{\mathrm{up}} + w_{\mathrm{down}}$ and $w_{\mathrm{up}} w_{\mathrm{down}}$ model b_{LCR} quite well, as shown in Table III. We thus take both of them into account and use the following linear combination: $b_{\mathrm{LCR}} = -0.0097 + 0.00066(w_{\mathrm{up}} + w_{\mathrm{down}}) + 0.00014(w_{\mathrm{up}} w_{\mathrm{down}})$, whose R-Square is 0.99. Similarly, a suitable model for c_{LCR} is found to be $c_{\mathrm{LCR}} = 0.042 - 0.0028(w_{\mathrm{up}} + w_{\mathrm{down}}) - 0.000072(w_{\mathrm{up}} w_{\mathrm{down}})$, whose R-Square is 0.99. Summarizing, the expression of LCR can be written as

$$\mathrm{LCR} = \begin{cases} 0.89 e^{[-0.0097 + 0.00066(w_{\mathrm{up}} + w_{\mathrm{down}}) + 0.00014(w_{\mathrm{up}} w_{\mathrm{down}})] R} & \\ \qquad -20\ \mathrm{dB} \le R \le 0\ \mathrm{dB} & \\ 0.89 e^{[0.042 - 0.0028(w_{\mathrm{up}} + w_{\mathrm{down}}) - 0.000072(w_{\mathrm{up}} w_{\mathrm{down}})] R} & \\ \qquad 0\ \mathrm{dB} < R \le 10\ \mathrm{dB} & \end{cases}. \quad (7)$$

The AFD can be computed as $\mathrm{CDF}(R)/\mathrm{LCR}(R)$[33], [34], where $\mathrm{CDF}(R)$ is the cumulative distribution function of the threshold level R. A simpler approximation can be obtained by fitting to the measured AFD. Analogous to the modeling LCR, the parameters of AFD (a_{AFD}, b_{AFD}, and c_{AFD}, similar to (6)) are obtained. Table III shows that none of the parameters of AFD can be modeled as a function of the structural parameters, therefore, the average values of them are chosen. Finally, AFD in the cutting scenario is expressed as

$$\mathrm{AFD} = \begin{cases} 0.45 e^{0.023 R} & -20\ \mathrm{dB} \le R \le 0\ \mathrm{dB} \\ 0.45 e^{0.52 R} & 0\ \mathrm{dB} < R \le 10\ \mathrm{dB} \end{cases}. \quad (8)$$

The validations of (7) and (8) are presented in Section V.

C. Amplitude Distribution

Even though there is clear LOS propagation in the cutting scenario, it is likely that the effects of reflection and scattering components are also very strong according to the preceding observations. The proportions of the components, such as direct, reflected, and scattered rays, are different from the traditional propagation scenario, and these proportions may change with distance. Consequently, the best fit distribution of amplitudes is entirely worthy of investigation.

To obtain a sufficient number of samples, we use the sliding/overlapped windows described above to conduct the distribution estimation, which allow a reasonable testing of the distribution fit and provide efficient tradeoff between the accuracy and complexity of the data processing. We use Akaike's Information Criteria (AIC) to select the model that best fits the empirical distribution of the fading amplitudes, among the four candidate distributions: Ricean, Nakagami, Rayleigh, and Lognormal. AIC is a measure of the relative goodness of fit of a statistical model and has found widespread use in wireless communications [35]–[37]. It asymptotically selects the model that minimizes the expected squared error between model and data [38]. The AIC for the j-th candidate distribution that has a probability density function, $g_{\hat{\theta}_j}$ is given by [35]

$$\mathrm{AIC}_j = -2 \sum_{n=1}^{N} \log_e [g_{\hat{\theta}_j}(x_n)] + 2U \quad (9)$$

where g is the probability density function (PDF) of the examined fading distribution, $\hat{\theta}_j$ is the maximum likelihood estimate of the distribution parameter vector θ_j obtained from the experiment data set, and U is the dimension of vector $\hat{\theta}_j$. N is the size of sample set $x = x_1, x_2 \cdots x_N$. The model with the lowest AIC provides the best fit. To conveniently compare the relative fit of each distribution within the candidate set, we define the AIC differences

$$\Phi_j = \mathrm{AIC}_j - \min_i \mathrm{AIC}_i \quad (10)$$

where $\min_i \mathrm{AIC}_i$ denotes the minimum AIC value over all J candidate families. Then we examine the candidates' relative fitting quality based on the Akaike weights w_j, defined as [35]

$$w_j = \frac{e^{-(1/2)\Phi_j}}{\sum_{i=1}^{J} e^{-(1/2)\Phi_i}} \quad (11)$$

where $\sum_{j=1}^{J} w_j = 1$. The model with the highest Akaike weights is the best distribution to describe the data set.

Fig. 5 shows the plots of the Akaike weights for different candidate distributions based on multiple measurements in five cuttings. It can be observed that the Ricean distribution has the best fit (the Akaike weights of the Ricean distribution function are

[9]To get a good model fit, we use 0 dB threshold as a break point, and (6) ensures the continuity at 0 dB threshold by default.

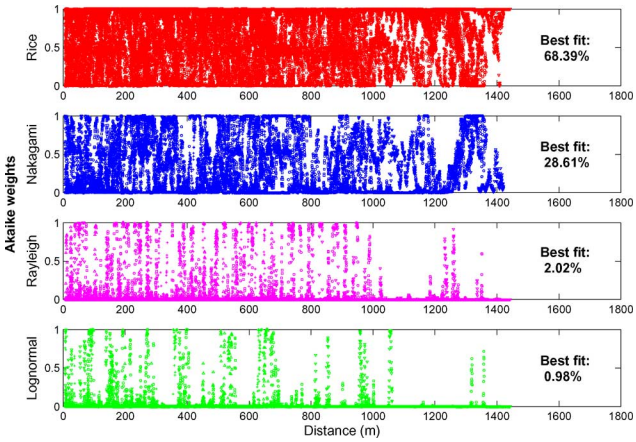

Fig. 5. Akaike weights and the percentage of the best fit for four candidate distributions based on multiple measurements. The measurements for cuttings Nos. 1, 2, 3, 4, and 5 are plotted with circles, squares, +'s, Δ's, and ∇'s, respectively.

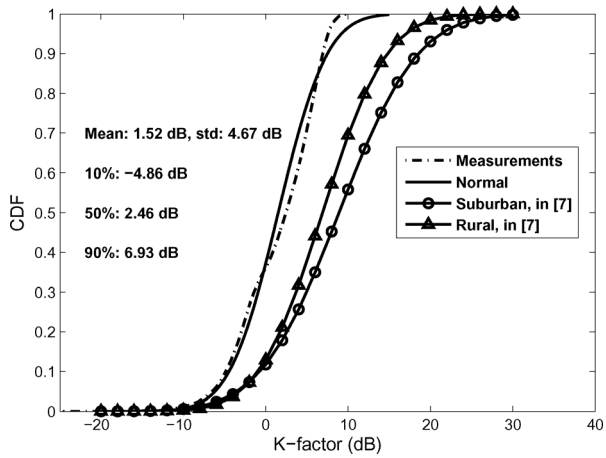

Fig. 6. Distribution of the K-factor over five cuttings (Nos. 1 to 5).

1 for most cases), and Nakagami is the second best. Rayleigh and Lognormal fits are not suitable for cutting scenarios. This is as expected since there is a clear LOS path due to the high transmitting antennas in HSR cutting scenarios, and the Ricean distribution is commonly used to describe propagation channels with a dominant signal. Moreover, the percentage of the best fit for each candidate distribution is presented in Fig. 5. On average, the percentage of the instances that Ricean distribution offers the best fit is 68.39% of all measurements, and Nakagami is second with 28.61%. Note that the Rayleigh distribution only offers the best fit for 2.02%, which means that even though there are rich reflection and scattering components, the fading in the cutting channel is not as severe as in a Rayleigh channel.

D. Ricean K-Factor Analysis

Based on the above findings, a Ricean distribution is utilized to model the fading characteristics. The PDF can be expressed as

$$f(r) = \frac{2(K+1)r}{\Omega} \times \exp\left(-K - \frac{(K+1)r^2}{\Omega}\right) I_0\left(2\sqrt{\frac{K(K+1)}{\Omega}}r\right) \quad (12)$$

where r is the small-scale-fading amplitude, $I_0(\cdot)$ is the 0th order modified Bessel function of the first kind. $\Omega = \mathrm{E}[r^2]$ and $\mathrm{E}[\bullet]$ denotes the expected value of $[\bullet]$. The parameter K is the Ricean K-factor, which is the power ratio of the dominant component (e.g., LOS) and scattered components. It is a measure of fading whose estimate is important in link budget calculations. We use the timesaving moment-based method in [39], [40] to estimate the Ricean K-factor, which can be expressed as

$$K = \frac{\sqrt{1 - \frac{\mathrm{Var}[r^2]}{(\mathrm{E}[r^2])^2}}}{1 - \sqrt{1 - \frac{\mathrm{Var}[r^2]}{(\mathrm{E}[r^2])^2}}} \quad (13)$$

where $\mathrm{Var}[\bullet]$ denotes the variance of $[\bullet]$. The K-factors extracted from the data of the sliding/overlapped windows described above are modeled to reflect the following variations: i) the ensemble variation of the K-factor over cases 1 to 5; ii) the variation of the K-factor against distance; and iii) the autocovariance function of the deviation of the K-factors from the linear K-factor model.

First, we conduct an ensemble examination of the K-factor over all measurement windows in the five cuttings. The CDF of the K-factor is shown in Fig. 6 and is found to be very nearly Gaussian. The mean value of the K-factor is 1.52 dB and the standard deviation is 4.67 dB. In addition, even though the AIC test rarely gives the Rayleigh distribution as the optimum distribution, the K-factors are often found to be small enough to allow description of the fading as Rayleigh. In contrast, the measurements in [7] are plotted in Fig. 6 for comparison, which shows that the K-factor in suburban/rural environments is up to 10 dB. The small K-factor in the HSR cutting scenario is caused by the strong reflected and scattered components from the sidewalls.

Second, we consider the K-factor as a function of distance for each cutting, and examine its variation trend. Our model consists of a distance-dependent mean of K-factor K_{mean} (which is based on the multiple measurements) and a standard deviation, expressed as

$$K_{\mathrm{dB}}(d,i) = K_{\mathrm{mean,dB}}(d,i) + x\sigma(i) \quad (14)$$

where x is a zero-mean Gaussian variable of unit standard deviation $N[0,1]$, σ is standard deviation, and i denotes the i-th cutting.

The estimated K_{mean}'s for each cutting are shown in Fig. 7. According to the visual observation, K_{mean} generally increases with the distance d when $d \leq 200$ m, and decreases with d when $d > 200$ m. In fact, $d = 200$ m can be approximately considered as a break point.[10] This observation can be explained as follows:

- When $d \leq 200$ m, the MS is close to the bottom of the base station and is not in the mainlobe of the directional base station antenna pattern, thus it receives the LOS component with considerable attenuation. This consequently leads to a more severe fading in this region, i.e., the K-factor is very small. The reduction of the LOS component is stronger the

[10]The location of break point is specific to the employed antennas, the positions and heights of base stations. A more general investigation would require the ability to change base station height and antenna pattern, which is not feasible in the HSR system in which we were allowed to do our measurements.

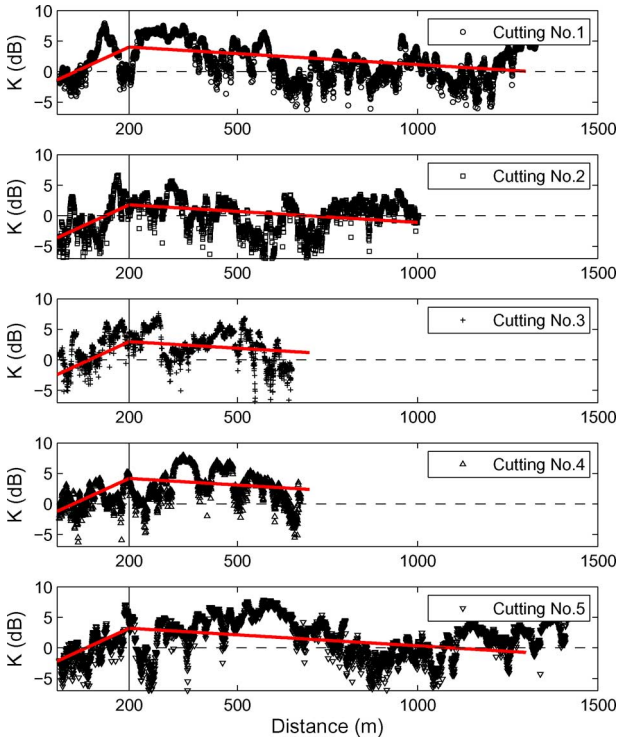

Fig. 7. Estimated K_{mean}'s based on repeated measurements. For clarity, we plot each case separately. The red curves are the proposed K_{mean} model of (17).

closer the MS is to the base station. Note that this area has not been considered by our previous work [27].

- When $d > 200$ m, the strength of the scattered component, which is the result of rays coming from a multiplicity of directions, will vary far less than the strength of the fixed component, which is dominated by rays coming from the direction of the base station (this phenomenon has been reported by [25] in suburban macrocells). Thus, K decreases with increasing d. This result is similar to the observation in [27].

According to Fig. 7, we use the following piecewise-linear formulation, which ensures the continuity of the model at 200 m, to model the distance-dependent K_{mean}

$$K_{\mathrm{mean}}(\mathrm{dB}) = \begin{cases} k_1(d-200)+k_2 & 0 < d \le 200 \text{ m} \\ k_3(d-200)+k_2 & 200 \text{ m} < d < 1500 \text{ m} \end{cases}. \tag{15}$$

The results of k_1's, k_2's, and k_3's are summarized in Table II. We use the statistical method in Fig. 3 to model k_1, k_2, and k_3. Table III shows that none of the structural parameters indicate a good fit for k_1 and k_3, so we use the mean value thereof: $\bar{k}_1 = 0.027$ and $\bar{k}_3 = -0.0036$. Note that constant k_3 is different from the expression in our previous work [27]. This is because the slopes of different cuttings in Fig. 7 are very small and close to each other when $d > 200$ m[11]. As for k_2, $w_{\mathrm{up}} + w_{\mathrm{down}}$ indicates a good fit and this can be expressed as

$$k_2 = 0.41(w_{\mathrm{up}} + w_{\mathrm{down}}) - 25.38. \tag{16}$$

Summarizing, the proposed piecewise-linear K_{mean} model can be written as

$$K_{\mathrm{mean}}(\mathrm{dB}) = \begin{cases} 0.027d + 0.41(w_{\mathrm{up}} + w_{\mathrm{down}}) - 30.78 & d \le 200 \text{ m} \\ -0.0036d + 0.41(w_{\mathrm{up}} + w_{\mathrm{down}}) - 24.66 & d > 200 \text{ m} \end{cases}. \tag{17}$$

Equation (17) offers a detailed variation trend of K_{mean} against distance and is plotted in Fig. 7. It shows that a larger value of $w_{\mathrm{up}} + w_{\mathrm{down}}$ leads to a higher K-factor. In other words, a "wide" cutting (with wide crown and bottom widths) helps to reduce the severity of fading – which is intuitive.

The standard deviation σ of the estimated K-factors against K_{mean} are extracted and summarized in Table II. Similarly, the break point at 200 m is utilized in the modeling of σ. We follow the method in Fig. 3 and get the model of σ from Table III, as follows:

$$\sigma(\mathrm{dB}) = \begin{cases} 4.45 & d \le 200 \text{ m} \\ -0.033(w_{\mathrm{up}} - w_{\mathrm{down}}) + 5.76 & d > 200 \text{ m} \end{cases}. \tag{18}$$

Note that the ensemble examination of the K-factor in Fig. 6 is more for comparison with other measurements in the literature, while for simulation purposes, the distance-dependent model of (14) should be used.

Third, we investigate the second-order statistic of the K-factor. For the i-th cutting, the deviation of the extracted K-factor from the linear K_{mean} model can be written as

$$\Delta K(d,i) = K(d,i) - K_{\mathrm{mean}}(d,i). \tag{19}$$

Then, we define the autocovariance function of $\Delta K(d,i)$ as shown in (20) at the bottom of the page, where Δd indicates distance difference. The second-order statistic $\rho(\Delta d, i)$ determines the correlation of the extracted $\Delta K(d,i)$. Furthermore, we consider the coherence length L_c, which is the minimum separation distance that satisfies the equation $\rho(L_c, i) \le 0.5$. A short L_c indicates that the K-factor changes quickly as the MS moves.

Fig. 8 shows the autocovariance function for five cuttings based on the averaging of repeated measurements. It can be noted that the autocorrelation function decays faster for $d \le 200$ m than for $d > 200$ m. The values of L_c are summarized in Table IV in terms of wavelength. Note that since we use a window size of 40 wavelengths, only the coherence length

[11]Comparing to our previous work [27], we use more measurements in this paper to improve the accuracy. In the following Section V, the proposed model is found to be well-suited to reproduce measured results.

$$\rho(\Delta d, i) = \frac{\mathrm{E}\{[\Delta K(d,i) - \mathrm{E}(\Delta K(d,i))][\Delta K(d+\Delta d, i) - \mathrm{E}(\Delta K(d+\Delta d, i))]\}}{\sqrt{\mathrm{Var}[\Delta K(d,i)]}\sqrt{\mathrm{Var}[\Delta K(d+\Delta d, i)]}} \tag{20}$$

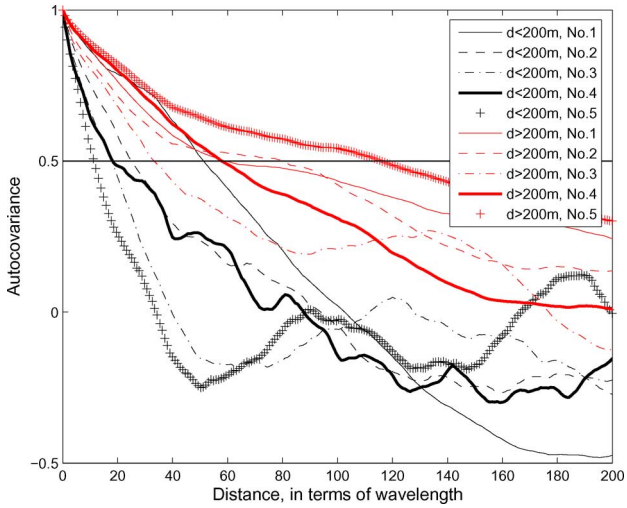

Fig. 8. Autocovariance functions. The solid line indicates $\rho = 0.5$.

TABLE IV
COHERENCE LENGTH FOR EACH CUTTING

Cutting Number	No.1	No.2	No.3	No.4	No.5	Mean Value
Coherence length L_c (wavelength) $d \leq 200$ m	52	<40	<40	<40	<40	<42
Coherence length L_c (wavelength) $d > 200$ m	59	79	<40	58	116	<70

larger than 40 wavelengths can be accurately observed. We thus use "< 40" in Table IV to represent those observed coherence lengths that are less than 40 wavelength. It shows that L_c is less than 42λ for $d \leq 200$ m and less than 70λ for $d > 200$ m. The higher value of L_c for $d > 200$ m is caused by the dominant LOS path.

V. MODEL VALIDATION

To validate our proposed models, we took additional measurements in cutting No. 6 to collect sufficient data for the model validation. The parameters of cutting No. 6 are summarized in Table I. In the following, the proposed models of LCR, AFD, and distance-dependent K_{mean} are compared to measurements in cutting No. 6 and other existing work (either theoretical results or empirical models).

Considering that the Ricean distribution is the optimal choice, the theoretical formulations developed from Clarke's isotropic scattering model are utilized to validate the LCR and AFD models, given as [33], [41]

$$\text{LCR} = r\sqrt{2\pi(K+1)}f_m e^{-K-(K+1)r^2} I_0(2r\sqrt{K(K+1)}) \tag{21}$$

$$\text{AFD} = \frac{1 - Q\left(\sqrt{2K}, \sqrt{2(K+1)r^2}\right)}{r\sqrt{2\pi(K+1)}f_m e^{-K-(K+1)r^2} I_0(2r\sqrt{K(K+1)})} \tag{22}$$

where r is the threshold voltage normalized to the r.m.s. envelope, $I_0(\cdot)$ is the zero order modified Bessel function of the first kind, $Q(\cdot)$ is the Marcum-Q function, and f_m is the maximum Doppler frequency. K-factors in (21) and (22) are in linear units. The normalized LCR and AFD expressions are utilized in the validation, i.e., LCR/f_m and $\text{AFD}f_m$ are plotted in Fig. 9 in terms of $20\log_{10}(r)$. For easy comparison, the theoretical results of Rayleigh fading ($K = -\infty$ dB) and the fading in suburban/rural environments [7] ($K \approx 10$ dB) are plotted.

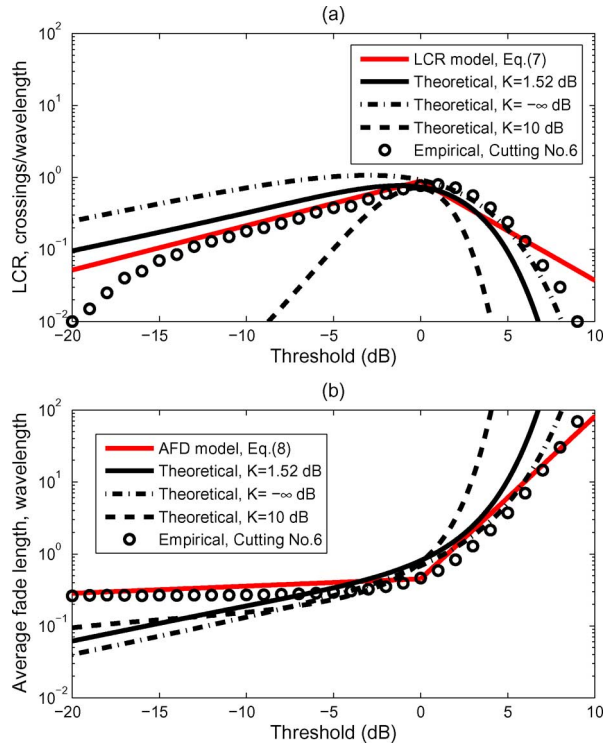

Fig. 9. Validation of LCR and AFD models using the measurements in cutting No. 6. The LCR values are normalized and given in terms of crossings per wavelength, and the AFD values are normalized and presented in wavelengths.

Fig. 9(a) shows the validation of LCR. Generally, reasonable agreement between measurements and the proposed model can be observed, except for the very low and high levels. The theoretical results calculated using the estimated K-factor (at 1.52 dB) are slightly higher than the proposed models when $R \leq 0$ dB. It is noteworthy that the theoretical result for $K = 1.52$ dB (which is the mean value of K as shown in Fig. 6) are close to the theoretical result with $K = -\infty$ dB, which means that the fading in cutting channel is close to the Ricean fading with a low K-factor. The theoretical result with $K = 10$ dB indicates fewer crossings, which means that the fading in the HSR cutting scenario is more severe than in the standard suburban/rural scenarios. Fig. 9(b) shows the validation of AFD. It is found that the proposed model and measurements are in reasonable agreement.

The disagreement between the measurements/proposed models and the theoretical result in Fig. 9 is mainly due to that (21) and (22) are based on an assumption that the diffuse components are isotropically indicant from all azimuth directions. However, such isotropic angle distribution will generally not hold in HSR cutting scenarios, as typically the base station antennas are directional and a long train (with the receiver mounted on the front part of the train) is placed in the cutting. Fig. 9 shows

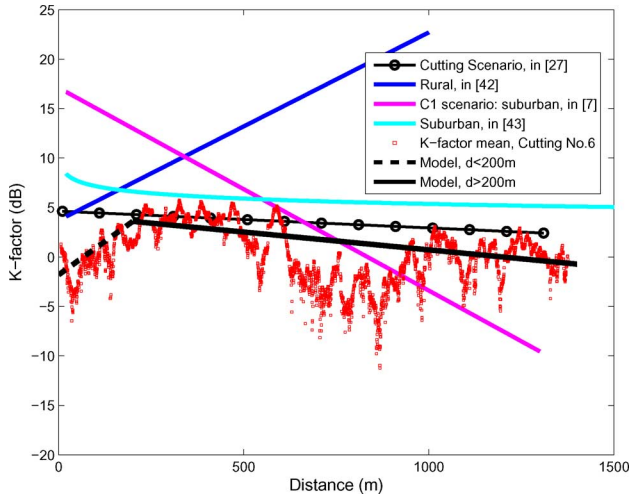

Fig. 10. K_{mean} model validation. The black dashed and solid lines represent the proposed piecewise models, using the structural parameters of cutting No. 6. The red squares are the mean values of K-factors.

that our proposed models can be used for predicting the LCR and AFD in the non-isotropic cutting channel.

To validate the K_{mean} model, we extract the K-factors from the measurements of cutting No. 6 using the same method in Section IV. The results of measured K-factors are compared to the proposed K_{mean} model, as shown in Fig. 10. It shows that the proposed K_{mean} model and measurements are well in agreement. Moreover, we present a comparison between (17) and some classical K-factor models shown in (23) at the bottom of the page. Fig. 10 shows that none of the existing models can be used for the K-factor estimation in the cutting scenario: the statistical models in [7], [27], and [43] lead to large prediction errors for the distance $d < 200$ m; and the model in [42] also shows poor performance in the cutting scenario. The errors of the former statistical models result from the special structure of the cutting scenario (which leads to rich reflection and scattering components in the cutting), and are partially due to the different carrier frequencies and antenna heights in the measurements.

In addition, it is noteworthy that all of these previous findings show that the K-factor is a monotone function of distance (as shown in Fig. 10). By contrast, our analysis shows that the trend of the K-factor changes from increasing to decreasing, at a break point around 200 m. This is because the cuttings give rise to rich reflection and scattering components, and the HSR system uses the particular directional transmitting antennas.

VI. Discussion

A. Structural Parameters

In general, there are three structural parameters in the cutting scenario: w_{up}, w_{down}, and depth H. Preceding observations show that the combinations of w_{up} and w_{down} affect the fading behavior much more significantly compared with individual w_{up} and w_{down}. This is because the cutting is like a large container that contains rich reflection and scattering components. When the steep walls on both sides are far from the receiver, reflected and scattered rays will be sharply attenuated by dissipation, and most of them have a higher possibility of leaving the cutting. $w_{\mathrm{up}} + w_{\mathrm{down}}$ and $w_{\mathrm{up}} w_{\mathrm{down}}$ can more adequately describe the distance from the steep walls to the receiver[12] and thus measure how well a cutting retains the multipath. These facts are reflected in the proposed models of (5) and (17), which demonstrate that "wide" cuttings (i.e., with both wide crown and bottom widths) are conducive to the reduction of the severity of fading.

In this paper, we considered four simple combinations of w_{up} and w_{down}: addition, subtraction, multiplication, and division. Some complex functions combining w_{up} and w_{down} are not examined. This is because the number of samples of the structural parameters used for modeling is quite limited. We just have five different cuttings for the parameterization, which is not enough to calculate the undetermined coefficients for a complex function.

B. Depth of Cutting

In [27], cuttings are divided into "deep" and "shallow" cuttings. The depth H is found to be influential in radio wave propagation. In fact, shallow cuttings do exist in HSR environments. But they are mostly used as transitions from deep cuttings to open areas, which usually results in the shallow cuttings being very short and with a height that changes substantially. The height (H) in this paper is typical for the implementation of HSR. Systematic investigations of the height dependence with sufficient number of samples to give statistically relevant results would be a task for future research.

C. Cross-Bridge in Cutting

It is common that cross-bridges are built over the cuttings to ensure necessary transportation for people around the HSR, as shown in Fig. 2. The cross-bridge in the cutting leads to non-line-of-sight (NLOS) propagation at a short distance, and causes an extra large-scale loss of about 5 dB [14], [26]. This larger scale variation of the signal may lead to poor coverage and handover failure. However, there is no obvious change of the small-scale-fading behavior caused by the cross-bridge from our preceding observations. The Ricean K-factor in Fig. 7 does show some drops at several locations, however, these drops do

[12]The distance from the steep walls to the receiver indicates the "average" distance to measure how far "on average" the steep wall is from the receiver. Only when both w_{up} and w_{down} are large, the "average" distance is large. Therefore, $w_{\mathrm{up}} + w_{\mathrm{down}}$ and $w_{\mathrm{up}} w_{\mathrm{down}}$ are good measures of the "average" distance.

$$K(\mathrm{dB}) = \begin{cases} (-0.0014 w_{\mathrm{down}} + 0.019)d + 4.63 & \text{Cutting, at 930 MHz, in [27]} \\ 0.019d + 3.7 & \text{Rural, at 5.25 GHz, in [42]} \\ -0.0205d + 17.1 & \text{Suburban, at 5.25 GHz, in [7]} \\ -1.8\log_{10}(0.001d) + 5.36 & \text{Suburban, at 2.5 GHz, in [43]} \end{cases} \tag{23}$$

not correspond to the locations of the cross-bridges. The variation of K-factor is much more affected by the condition of reflection and scattering than the temporary NLOS. In addition, the width of the cross-bridges is generally less than 5 m. For a high-speed moving train, this temporary change from LOS to NLOS cannot significantly affect the fading behavior at the receiver.

D. Surrounding Obstacles Outside the Cutting

Based on the proposed statistical models, there is no distinct difference of fading behavior between deep cuttings in suburban areas (Nos. 1 and 5) and that in rural areas (Nos. 2, 3, and 4). This is because the receiver on the train is lower than the top of the cutting, thus making it difficult for the reflected rays from the surrounding obstacles outside the cutting to reach the receiver. The special structure, and the rich reflection and scattering components in the cutting provide the dominant impact on small-scale fading. Consequently, the surrounding obstacles outside the cutting are negligible in the fading analysis.

VII. Conclusion

In this paper, we analyzed wireless propagation for HSR, in particular the small-scale fading in cutting scenarios. Considering the special structure, rich reflection and scattering components, extreme severity of fading, and widespread use in HSR, this is very important for system design.

First, we described the collection of a large body of data at 930 MHz for cutting scenarios in the "Zhengzhou-Xi'an" HSR of China. We gave full consideration to special structures in measurements and analysis. Six cuttings with different structures were studied, which cover the typical scenarios of HSR. For the temporal variations of channel, we found that the FD is around 17 dB; at -10 dB threshold level, the LCR is around 0.21 per wavelength, and the AFD is around 0.34 wavelengths. We proposed a set of effective methods to examine the impact of structure on fading parameters and to model them statistically.

Then, we extensively investigated the small-scale amplitude fading distribution. An AIC-based method was applied to select the distribution function that best describes the channel variation. The Ricean function was identified to be the most suitable model to describe the amplitude variations for the overall cutting channel. However, the ensemble K-factor of Ricean distribution is very low at 1.52 dB due to the rich scattering components, which means that the fading in cuttings is more severe than the other LOS scenarios. We presented a novel piecewise K-factor model (with a break point around 200 m) over distance, which is a result of the weak LOS component near the base station caused by the directional transmitting antennas. The proposed model was validated through the measurements in the sixth cutting, and found to be more accurate than some classical K-factor models. Furthermore, the autocovariance function of the deviation of the extracted K-factors from the proposed model was presented and the coherence length was found to be less than 42λ and less than 70λ for the areas before and after break point. In addition, the proposed LCR and AFD models were validated by comparing to the theoretical results and the measurements.

Finally, we found that it is more difficult for a "wide" cutting (i.e., with both large w_{up} and large w_{down}) to retain the reflection and scattering components. This means even though a cutting is a scenario with severe fading, a "wide" cutting tends to reduce the severity of fading. The surrounding obstacles outside the cutting have a marginal impact on fading behavior. In addition, the effect of the cross-bridge was found to be negligible in the fading analysis. The results of our research provide some insights of the fading behavior in HSR cutting channel, and can be helpful to those engaged in designing HSR communication systems.

Appendix

Model Selection: We choose the five functions based on the following principles:

1) The regression fit can be improved by a model with more parameters, however, the *principle of parsimony*[44] suggests that a model should have the smallest possible number of parameters for adequate representation of the data. Therefore, we choose the models with two parameters, which is generally the least dimension of the model for a practical fitting [38].
2) Considering the limited size of the samples for the parameterization, the estimation for the complex non-monotonic models cannot get a sufficient accuracy [45]. Therefore, only the monotonic models will be chosen. By the same token, only the low-order models, e.g., first-order polynomial, will be chosen.

Summarizing, we find that the models in the *First* step should: i) have a small number of parameters (i.e., 2 parameters); and ii) be monotonic and the order is low. Therefore, we choose the following five functions: $v = a\log_{10}(w) + b$, $v = a\sqrt{w} + b$, $v = aw + b$, $v = a(w)^2 + b$, and $v = ae^{bw}$, which cover all the important classes of functional growth. The model validation in Section V shows that the accuracy of the proposed models based on these five functions is sufficient.

Goodness-of-Fit Evaluation: To evaluate the goodness of fit, three GoF statistics for parametric models are employed [46]: SSE, R-Square, and RMSE.

SSE: This statistic is a measure of the discrepancy between the data and an estimation model, and is expressed as

$$\mathrm{SSE} = \sum_{i=1}^{n} w_i (y_i - \hat{y}_i)^2 \tag{24}$$

where y_i is the raw data, $\hat{y}_i$ is the estimate of raw data, and n is the total number of raw data. w_i indicates the weight of y_i and is chosen as $w_i = 1/n$ in our calculation. A small SSE close to 0 indicates a tight fit of the model to the data.

R-Square: This statistic is called the coefficient of determination and it measures how successful the fit is in explaining the variation of the data. R-Square is defined as the ratio of the sum of squares of the regression (SSR) and the total sum of squares (TSS). It is expressed as

$$\mathrm{R-Square} = \frac{\mathrm{SSR}}{\mathrm{TSS}} = \frac{\sum_{i=1}^{n} w_i (\hat{y}_i - \bar{y})^2}{\sum_{i=1}^{n} w_i (y_i - \bar{y})^2} \tag{25}$$

where $\bar{y}$ is the mean value of raw data. R-Square ranges from 0 to 1, with a value closer to 1 indicating that the regression model fits the data better.

RMSE: This statistic is a frequently used measure of the differences between values predicted by a model and the values actually observed. It is defined as

$$\mathrm{RMSE} = \sqrt{\frac{\mathrm{SSE}}{n-m}} \tag{26}$$

where m is the number of fitted coefficients estimated from the raw data. Just as with SSE, an RMSE value closer to 0 indicates a fit that is more useful for prediction.

In the *First* step of Section III, we first use the GoF to select one suitable $\tilde{F}_{\hat{j}(i)}(w_i)$ for each w_i from the five fitting functions, where the $\tilde{F}_{\hat{j}(i)}$ that gives the maximum R-Square and minimum SSE/RMSE is selected for each w_i. Then we further test whether $\tilde{F}_{\hat{j}(i)}(w_i)$ passes the GoF test in an absolute sense (i.e., leads to a result that the GoF test accepts): the $\tilde{F}_{\hat{j}(i)}(w_i)$ that gives a R-Square larger than 0.5 is accepted. The threshold of 0.5 in our work is based on the LMSE implementation and the visual observation of the fit curves. Note that the suitable threshold of R-Square generally depends on the object of study, and a threshold of 0.5 is widely considered acceptable [45]. In fact, the values of R-Square of our proposed models in this paper are mostly larger than 0.7, which indicates satisfactory fit.

ACKNOWLEDGMENT

The authors are grateful to Prof. L. J. Greenstein, Prof. G. D. Durgin, Prof. P. Marinier, and Dr. G. Wang for the useful discussion which stimulated this paper. The authors also wish to express their appreciation to L. Chen, B. Mi, X. Ding, and L. Zhao, for their help to perform the propagation measurements. We thank the anonymous reviewers for their thorough reading and constructive comments, which greatly helped to improve the paper.

REFERENCES

[1] R. He, Z. Zhong, B. Ai, J. Ding, and Y. Yang, "Propagation measurements and analysis of fading behavior for high speed rail cutting scenarios," in *Proc. IEEE Globecom*, 2012, pp. 5237–5242.

[2] W. T. Webb and R. D. Shenton, "Pan-European railway communications: where PMR and cellular meet," *J. Inst. Electr. Eng. Electron. Commun. Eng.*, vol. 6, pp. 195–202, 1994.

[3] M. Goller, "Application of GSM in high speed trains: measurement and simulations," in *Inst. Electr. Eng. Colloq. Radio Commun. Transport.*, 1995, pp. 5/1–5/7.

[4] M. Goller, "Radio channel measurements in lines of German railway (Deutsche Bundesbahn) in the 900 MHz frequency band," in *Proc. COST231*, 1992, vol. TD(92)20, pp. 7–10.

[5] M. Goller, K. Masur, G. Frohlingsdorf, and U. Weber, "Measurement results and parameters for modelling mobile railway radio channels in the 900 MHz band," *Nachrichtentechnik Elektronik*, vol. 43, no. 6, pp. 290–295, 1993.

[6] M. Uhlirz, "Adapting GSM for use in high-speed railway networks," , Institut fiir Nachrichtentechnik und Hochfrequenztechnik Technische Universitiit Wien, Wein, 1995.

[7] P. Kyosti *et al.*, "WINNER II channel models," *WINNER II Public Deliverable*, pp. 158–169, Sep. 2007.

[8] Y. Okumura, E. Ohmori, T. Kawano, and K. Fukua, "Field strength and its variability in UHF and VHF land-mobile radio service," *Rev. Electron. Commun. Lab.*, vol. 16, no. 9, 1968.

[9] M. Hata, "Empirical formula for propagation loss in land mobile radio services," *IEEE Trans. Veh. Technol.*, vol. VT-29, no. 3, pp. 317–325, Aug. 1980.

[10] R. He, Z. Zhong, B. Ai, and J. Ding, "An empirical path loss model and fading analysis for high-speed railway viaduct scenarios," *IEEE Antennas Wireless Propag. Lett.*, vol. 10, pp. 808–812, 2011.

[11] R. He, Z. Zhong, B. Ai, G. Wang, J. Ding, and A. F. Molisch, "Measurements and analysis of propagation channels in high-speed railway viaducts," *IEEE Trans. Wireless Commun.*, to be published.

[12] R. He, Z. Zhong, and B. Ai, "Path loss measurements and analysis for high-speed railway viaduct scene," in *Proc. 4th Int. Wireless Commun. Mob. Comput. Conf.*, France, 2010, pp. 266–270.

[13] R. He, Z. Zhong, B. Ai, and J. Ding, "Measurements and analysis of short-term fading behavior for high-speed rail viaduct scenario," in *Proc. IEEE ICC*, 2012, pp. 4563–4567.

[14] F. Abrishamkar and J. Irvine, "Comparison of current solutions for the provision of voice services to passengers on high speed trains," in *Proc. IEEE 52nd Veh. Technol. Conf.*, 2000, pp. 2068–2075.

[15] M. Lienard and P. Desaugue, "Characterization of the propagation channel in a high speed train environment," in *Proc. IEEE 9th MELECON*, 1998, pp. 260–262.

[16] M. Lienard and P. Degauque, "Propagation in wide tunnels at 2 GHz: a statistical analysis," *IEEE Trans. Veh. Technol.*, vol. 47, no. 4, pp. 1322–1328, Apr. 1998.

[17] D. J. Cichon, T. Zwick, and W. Wiesbeck, "Ray optical modeling of wireless communications in high-speed railway tunnels," in *Proc. IEEE 46th Veh. Technol. Conf.*, 1996, pp. 546–550.

[18] M. Lienard, S. Betrencourt, and P. Degauque, "Theoretical and experimental approach of the propagation at 2.5 GHz and 10 GHz in straight and curved tunnels," in *Proc. IEEE 50th Veh. Technol. Conf.*, 1999, pp. 2268–2271.

[19] P. Aikio, R. Gruber, and P. Vainikainen, "Wideband radio channel measurements for train tunnels," in *Proc. IEEE 48th Veh. Technol. Conf.*, 1998, pp. 460–464.

[20] A. F. Molisch, *Wireless Communications*, 2nd ed. New York, NY, USA: IEEE-Wiley, 2011.

[21] T. S. Rappaport, *Wireless Communications Principles and Practice*, 2nd ed. Englewood Cliffs, NJ, USA: Prentice-Hall, 2001.

[22] W. C. Y. Lee, *Mobile Communications Engineering*. New York, NY, USA: McGraw-Hill, 1993.

[23] H. Hashemi, M. McGuire, T. Vlasschaert, and D. Tholl, "Measurements and modeling of temporal variations of the indoor radio propagation channel," *IEEE Trans. Veh. Technol.*, vol. 43, no. 3, pp. 733–737, Aug. 1994.

[24] P. Marinier, G. Y. Delisle, and C. L. Despins, "Temporal variations of the indoor wireless millimeter-wave channel," *IEEE Trans. Antennas Propag.*, vol. 46, no. 6, pp. 928–934, Jun. 1998.

[25] L. J. Greenstein, S. S. Ghassemzadeh, V. Erceg, and D. G. Michelson, "Ricean K-factors in narrowband fixed wireless channels: Theory, experiments, and statistical models," *IEEE Trans. Veh. Technol.*, vol. 58, no. 8, pp. 4000–4012, Oct. 2009.

[26] J. Lu, G. Zhu, and C. Briso, "Fading characteristics in the railway terrain cuttings," in *Proc. IEEE 73rd Veh. Technol. Conf.*, 2011, pp. 1–5.

[27] R. He, Z. Zhong, B. Ai, and J. Ding, "Propagation measurements and analysis for high-speed railway cutting scenario," *Electron. Lett.*, vol. 47, no. 21, pp. 1167–1168, Oct. 2011.

[28] W. C. Y. Lee, "Estimate of local average power of a mobile radio signal," *IEEE Trans. Veh. Technol.*, vol. VT-34, no. 1, pp. 22–27, Feb. 1985.

[29] B. Ai, Z. Zhong, G. Zhu, and M. Zhao, "Novel statistical criteria for local mean power estimation in wireless coverage prediction," *IET Microw. Antennas Propag.*, vol. 5, no. 5, pp. 596–604, 2011.

[30] B. Ai, Z. Zhong, G. Zhu, and J. Liu, "Novel statistical processing methods for wireless field strength prediction," *IEEE Trans. Consum. Electron.*, vol. 55, no. 4, pp. 1805–1809, 2009.

[31] S. Kozono, "Received signal-level characteristics in a wide-band mobile radio channel," *IEEE Trans. Veh. Technol.*, vol. 43, no. 3, pp. 480–486, Aug. 1994.

[32] J. D. Parsons, *The Mobile Radio Propagation Channel*. Chichester, U.K.: Wiley, 2000.

[33] A. Abdi, K. Wills, H. A. Barger, M. S. Alouini, and M. Kaveh, "Comparison of the level crossing rate and average fade duration of Rayleigh, Rice and Nakagami fading models with mobile channel data," in *Proc. IEEE VTC*, 2000, pp. 1850–1857.

[34] R. Feick, R. A. Valenzuela, and L. Ahumada, "Experimental results on the level crossing rate and average fade duration for urban fixed wireless channels," *IEEE Trans. Wireless. Comm.*, vol. 6, no. 1, pp. 175–179, 2007.

[35] U. G. Schuster and H. Bölcskei, "Ultrawideband channel modelling on the basis of information-theoretic criteria," *IEEE Trans. Wireless Commun.*, vol. 6, no. 7, pp. 2464–2475, Jul. 2007.

[36] S. Wyne, A. P. Singh, F. Tufvesson, and A. F. Molisch, "A statistical model for indoor office wireless sensor channels," *IEEE Trans. Wireless Commun.*, vol. 8, no. 8, pp. 4154–4164, Aug. 2009.

[37] X. H. Mao, Y. H. Lee, and B. C. Ng, "Statistical modeling of signal variation for propagation along a lift shaft," *IEEE Antennas Wireless Propag. Lett.*, vol. 9, pp. 752–755, 2010.

[38] K. P. Burnham and D. R. Anderson, *Model Selection and Multimodel Inference: A practical Information-Theoretic Approach*, 2nd ed. New York, NY, USA: Springer, 2002.

[39] L. J. Greenstein, D. G. Michelson, and V. Erceg, "Moment-method estimation of the Ricean K-factor," *IEEE Commun. Lett.*, vol. 3, no. 6, pp. 175–176, Jun. 1999.
[40] A. Abdi, C. Tepedelenlioglu, M. Kaveh, and G. Giannakis, "On the estimation of the K parameter for the Rice fading distribution," *IEEE Commun. Lett.*, vol. 5, no. 3, pp. 92–94, Jul. 2001.
[41] G. L. Stuber, *Principles of Mobile Communications*, 2nd ed. Dordrecht, The Netherlands: Kluwer, 2001.
[42] A. F. Molisch, L. J. Greenstein, and M. Shafi, "Propagation issues for cognitive radio," *Proc. IEEE*, vol. 97, no. 5, pp. 787–804, May 2009.
[43] V. Erceg, P. Soma, D. S. Baum, and S. Catreux, "Multiple-input multiple-output fixed wireless radio channel measurements and modeling using dual-polarized antennas at 2.5 GHz," *IEEE Trans. Wireless. Comm.*, vol. 3, no. 6, pp. 2288–2298, 2004.
[44] G. E. P. Box and G. M. Jenkins, *Time Series Analysis: Forecasting and Control*. London, U.K.: Holden-Day, 1970.
[45] J. O. Rawlings, S. G. Pantula, and D. A. Dickey, *Applied Regression Analysis: A Research Tool*. New York, NY, USA: Springer Verlag, 1998.
[46] *Matlab Help Documentation*, [Online]. Available: http://www.mathworks.com/help/toolbox/curvefit/bq_6zzm.html

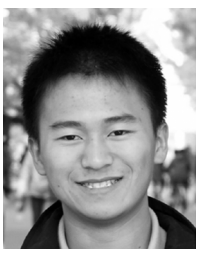

Ruisi He (S'11–M) received B.E. degree from School of Electronic and Information Engineering, Beijing Jiaotong University, Beijing, China, in 2009. Currently, he is working toward the Ph.D. degree in State Key Laboratory of Rail Traffic Control and Safety & School of Electronic and Information Engineering, Beijing Jiaotong University.

In 2010, he was a Vsiting Scholar in Universidad Politécnica de Madrid, Madrid, Spain. From 2012 to 2013, he has been a Research Scholar with the Department of Electrical and Engineering, University of Southern California, Los Angeles, CA, USA. His current research interests are in the field of measurement and modeling of wireless propagation channels, high-speed railway communications, and vehicle-to-vehicle communications.

He has authored/co-authored over 20 research papers in international journals and conferences, and he received the Best Paper Award in IEEE ICGSIS, 2011.

Zhangdui Zhong is a professor and advisor of Ph.D. candidates in Beijing Jiaotong University, Beijing, China. He is now a director of School of Computer and Information Technology and a Chief Scientist of State Key Laboratory of Rail Traffic Control and Safety in Beijing Jiaotong University. He is also a director of the Innovative Research Team of Ministry of Education, and a Chief Scientist of Ministry of Railways in China. He is an executive council member of Radio Association of China, and a deputy director of Radio Association of Beijing. His interests are wireless communications for railways, control theory and techniques for railways, and GSM-R system. His research has been widely used in the railway engineering, such as Qinghai-Xizang railway, Datong-Qinhuangdao Heavy Haul railway, and many high-speed railway lines of China.

He has authored/co-authored 7 books, 5 invention patents, and over 200 scientific research papers in his research area. He received MaoYiSheng Scientific Award of China, ZhanTianYou Railway Honorary Award of China, and Top 10 Science/Technology Achievements Award of Chinese Universities.

Bo Ai (M'00–SM'10) received the M.S. and Ph.D. degrees from Xidian University, Xi'an, China, in 2002 and 2004, respectively. He graduated in 2007 with great honors of Excellent Postdoctoral Research Fellow in Tsinghua University, Beijung, China.

He is now working in Beijing Jiaotong University as a Professor and advisor of Ph.D. degree candidates. He is a Deputy Director of State Key Laboratory of Rail Traffic Control and Safety. He is an Associate Editor of IEEE TRANSACTION ON CONSUMER ELECTRONICS and an editorial committee member of the *Journal of Wireless Personal Communications*. He has authored/co-authored 6 books, 26 invention patents and 130 scientific research papers in his research area until now. His current interests are the research and applications OFDM techniques, HPA linearization techniques, radio propagation and channel modeling, GSM Railway systems. He is a Senior member of the Electronics Institute of China (CIE).

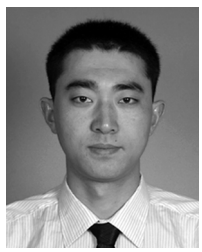

Jianwen Ding received B.S. and M.S. degrees from Beijing Jiaotong University, Beijing, China, in 2002 and 2005, respectively.

From 2005 to 2008, he was an Assistant in Beijing Jiaotong University. Since 2008, he has been working in Beijing Jiaotong University as a Lecturer.

Dr. Ding received second prize of progress in science and technology of Chinese Railway Society. His interests are broadband mobile communication and personal communication, dedicated mobile communication system for railway, and safety communication technology for train control system.

Yaoqing (Lamar) Yang (S'02–M'09–SM'09) received the B.S. degree from the Northern Jiaotong University, Beijing, China, in 1983, and the M.S. degree from the Beijing Broadcast Institute, Beijing, China, in 1986, both in electrical engineering. He received the Ph.D. degree in the area of wireless communications and networks from the University of Texas at Austin, Austin, TX, USA, in 2006.

He served as a Lecturer at the Beijing Broadcast Institute between 1986 and 1997. In August 1997, he was a Visiting Scholar with the University of Texas at Austin, where he worked on a semiconductor project. From 1999 to 2002, he worked as a Research Assistant on the Advanced Research Program (ARP) project for smart antenna measurements. Later, he developed a 4×8 wideband MIMO channel sounder that incorporated spread spectrum technology. He also worked as a Teaching Assistant from 2002 to 2005. In August 2006, he joined the faculty of the Department of Computer and Electronics Engineering, University of Nebraska-Lincoln (UNL), Lincoln, NE, USA. His current research interests lie in wireless communications and networks with emphasis on radio channel characterizations, cognitive radio networks, and statistical signal processing. Dr. Yang is a senior member of IEEE.

Andreas F. Molisch (S'89–M'95–SM'00–F'05) received the Dipl. Ing., Ph.D., and habilitation degrees from the Technical University of Vienna, Vienna, Austria, in 1990, 1994, and 1999, respectively.

He was with AT&T (Bell) Laboratories Research (USA); Lund University, Lund, Sweden, and Mitsubishi Electric Research Labs (USA). He is now a Professor of Eectrical Engineering with the University of Southern California, Los Angeles, CA, USA. His current research interests are the measurement and modeling of mobile radio channels, ultra-wideband communications and localization, cooperative communications, multiple-input-multiple-output systems, wireless systems for healthcare, and novel cellular architectures. He has authored, coauthored, or edited four books (among them the textbook Wireless Communications, Wiley-IEEE Press), 14 book chapters, some 150 journal papers, and numerous conference contributions, as well as more than 70 patents and 60 standards contributions.

Dr. Molisch has been an Editor of a number of journals and special issues, General Chair, Technical Program Committee Chair, or Symposium Chair of multiple international conferences, as well as Chairman of various international standardization groups. He is a Fellow of the AAAS, Fellow of the IET, an IEEE Distinguished Lecturer, and a Member of the Austrian Academy of Sciences. He has received numerous awards, most recently the James Evans Avant-Garde award of the IEEE Vehicular Technology Society, the Donald Fink Prize of the IEEE, and the Eric Sumner Award of the IEEE.